Distributed fiber optic sensing system for vibration monitoring of 3D printed bridges*

ZHAO Shuai[1,2], ZHOU Ran[1,2], LUO Mingming[1,2], LIU Jianfei[1,2], LIU Xiongfei[3], and ZHOU Tao[4]**

1. School of Electronic Information Engineering, Hebei University of Technology, Tianjin 300401, China

2. Tianjin Key Laboratory of Electronic Materials and Devices, Tianjin 300401, China

3. School of Civil Engineering and Transportation, Hebei University of Technology, Tianjin 300401, China

4. Tianjin Jinhang Institute of Technical Physics, Tianjin 300308, China

(Received 24 January 2024; Revised 8 August 2024)

The fiber optic sensing technology provides data support in structural health monitoring of the macro facilities, including design, construction, and maintenance of bridges, tunnels, ports and other infrastructures. In this paper, a distributed vibration sensing system is proved to be responsive to a single touch over a 1.8-m-long equivalent fiber segment, covering a vibration frequency from 5 Hz to 25 kHz. The sensing fiber was arranged as an S type layout on the bridge to recognize the standing state, windblown disturbance, and walking vibration. Moreover, the knocking and climbing events are recognized fiber laying spinning lines and hanging on the fences, respectively. The demonstration shows an accurate positioning and sensitive vibration monitoring applied on the automated three-dimensional (3D) printed bridge, which is applicable to all kinds of 3D printed facilities as intelligent sensory neuro-networks.

Document code: A **Article ID:** 1673-1905(2025)01-0028-7

DOI https://doi.org/10.1007/s11801-025-4027-7

1. Introduction

Three-dimensional (3D) printing technology essentially belongs to a rapid prototyping additive manufacturing process[1], which is based on digital model files and uses spraying, fusing, and sintering to build the structure of an object in 3D space[2]. Introducing this concept into the field of architecture, inorganic materials and adhesives can be used to create building frames, and high-strength fibers and concrete can be used for reinforcement and filling, and the model blueprints can finally be processed in layers and stacked to form the building[3,4]. Hebei University of Technology designed and manufactured an assembled concrete 3D-printed arch bridge over the approach river on the Beichen campus in 2019[5], which was certified as the longest 3D-printed bridge by the Guinness Book of World Records. However, the mechanical strength of 3D-printed buildings is weaker than that of ordinary concrete due to the limitation of the material ratio[6], and the different curing rates and surface evaporation are prone to produce peeling between the layered interfaces[5]. Drawing on the idea of curing crystal structures with microscopic graphite interlayer compounds (intercalators), MA et al[7] enhanced the ultimate tensile strength and shear strength in the cross-section direction with the help of U-pinning method, which improves the toughness and durability of the printed structure. 3D printing technology is applied to macroscopic constructions represented by bridges, which will subvert the traditional construction industry by virtue of its advantages of high automation, energy efficiency, and environmentally friendly, etc. However, the 3D printing technology has also brought about the need for a new construction process under the new building technology, and also brings worries and concerns about structural health monitoring under the new construction process.

The irregular vibration of the bridge originates from the vibration transverse wave transmitted by traveling vehicles, pedestrians and even wind loads[8], and its frequency depends on the force and microdeformation of the bridge deck caused by vehicle traveling. When the vibration frequency is close to the intrinsic frequency of the bridge, the resonance phenomenon will be generated, resulting in increased fluctuation of the bridge and causing safety hazards[9]. Electronic vibration sensing devices can be deployed in key locations of the bridge to obtain the bridge vibration information, but it is susceptible to interference from other electronic devices or external

* This work has been supported by the National Natural Science Foundation of China (No.6210031560), the Natural Science Foundation of Hebei Province (No.A2020202013), and the Natural Science Foundation of Tianjin City (No.21JCQNJC00780).

** LUO Mingming is an associate professor at the School of Electronic Information Engineering, Hebei University of Technology. He received his Ph.D. degree from Nankai University in 2016. His research interests are mainly in microstructured optical fiber, high spatial resolution distributed fiber optic sensing technology, micro-nano-scale microcavity lasers, and smart fiber optic sensing technology. E-mail: mmluo@hebut.edu.cn.

open electromagnetic fields, thus affecting its electromagnetic compatibility performance and measurement accuracy[10]. Electronic vibration sensors are mostly composed of metal components, and outdoor use is susceptible to sunlight and rain to accelerate corrosion and aging, requiring regular replacement or maintenance[11]. As a monitoring technology with high sensitivity, anti-electromagnetic interference, and distributed monitoring[12], fiber optic sensors have the ability to be widely used in extreme environments, complex electromagnetic interference, and other scenarios and maintain good stability and accuracy[13]. Implanted fiber Bragg grating (FBG) can provide real-time feedback on the structural health of bridge measurement points, but the single-point discrete sensors still cannot meet the demand for point-by-point distributed monitoring of large bridges[14]. Phase-sensitive optical time-domain reflectometer (φ-OTDR) is a long-distance, distributed, and highly sensitive vibration monitoring technology[15], which can realize real-time vibration monitoring along the optical fiber[16]. Its system structure is simple, easy to build and maintain, and can borrow redundant fiber cores from communication fiber optic cables, which is well adapted for bridge vibration monitoring[17,18].

In this paper, a distributed fiber-optic sensing system based on φ-OTDR is constructed and applied to 3D printed bridge of Hebei University of Technology for vibration monitoring. The precise spatial localization and vibration signal reduction performance are verified by piezoelectric ceramics (PZT), and the frequency response covers the range of 5 Hz—25 kHz. With the help of measurement optical fibers laid on the bridge deck, guardrail, and girder plate locations, the simultaneous positioning monitoring of spatial multi-point vibration was realized by simulating common disturbance behaviors such as knocking, climbing, walking, etc, and the equivalent spatial resolution accuracy of the system is 1.8 m. Distributed fiber optic intelligent sensing system is applied to 3D printed bridge vibration monitoring, which has good reliability and real-time performance, providing a new idea and new method for structural health monitoring of bridges.

2. Proposed structure

The φ-OTDR is a distributed fiber-optic sensing system based on backward Rayleigh scattering, which realizes the sensing of the environment by comparing the time-frequency characteristics of backward Rayleigh-scattered light excited by narrow linewidth pulses. As shown in Fig.1, when there is a perturbation near the sensing fiber, the phase and light intensity of the Rayleigh scattered light signal will be changed due to the elastic-optical effect and Poisson effect of the fiber. The phase modulation of the backward Rayleigh scattered light returned from the disturbance to the sensing fiber is a linear modulation, so the *I*/*Q* demodulation algorithm can be used to solve the phase of the backward Rayleigh scattered light signal and the time domain difference to get the position information of the external vibration signal, and the spatial coordinates of the peak of the difference signal are the position of the external disturbance source.

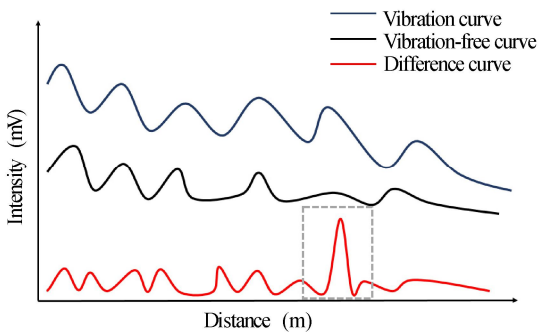

Fig.1 Positioning principle

The structure of the phase-sensitive optical time-domain reflection system is shown in Fig.2, in which a 3 kHz narrow linewidth low-frequency drifting laser emits 20 mW of continuous light with a wavelength of 1 550 nm, and splits the two optical signals with a power ratio of 90: 10 through a 3 dB coupler 1 (OC1). The optical signal with a power ratio of 90% is modulated by an acousto-optic modulator (AOM) into a 100 ns pulse with a re-frequency of 80 MHz, which is amplified by an erbium-doped fiber amplifier (EDFA) and then fed into the sensing fiber. The backward Rayleigh scattered signal returned from the sensing fiber is interfered by a circulator (CIR) with light of 10% power share of the principal oscillator in a 3 dB coupler 2 (OC2) with a splitting ratio of 50: 50, and is converted into an electrical signal and filtered out of the direct-current (DC) signal by a balanced photodetector (BPD). The signal is converted to an electrical signal by a BPD and filtered out as a DC signal. The signal is then converted to digital demodulation by a data acquisition card (DAQ) with a sampling rate of 250 Msps and transmitted back to the host computer. The clock signal output from the acquisition card controls the acousto-optic modulator drive for timing synchronization, ensuring the stability and accuracy of the measurement system.

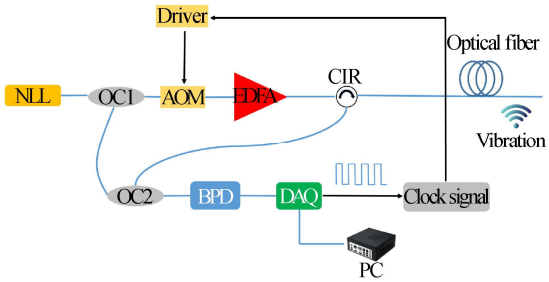

Fig.2 φ-OTDR system structure

3. Performance and experimental analysis

The demodulation of the signals is performed using a digital quadrature demodulation algorithm[19], and the

flowchart of the digital quadrature demodulation is shown in Fig.3. Firstly, the acquired digital signal $S(n)$ is cross-multiplied with a pair of orthogonal signals of the same frequency, $\cos(\Delta\omega_n n)$ and $\sin(\Delta\omega_n n)$, respectively, which are generated by the computer. Here, $\Delta\omega_n n$ refers to the angular frequency increment of the same frequency as the acquired signal $S(n)$ which is used to generate the orthogonal reference information, while n is the index of the time series, which indicates the discrete time point of the acquired signal. Next, the sum frequency signals are filtered by a low-pass filter to finally obtain a pair of orthogonal difference frequency signals I and Q. This process can be expressed by the following equation.

For the I signal, we have

$$Y_I = S(n)\times\cos(\Delta\omega_n n) = \frac{1}{2}E_s(n)E_o(n)\{\cos[2\Delta\omega_n n+\varphi_s(n)]+\cos\varphi_s(n)\}. \quad (1)$$

For the Q signal, we have

$$Y_Q = S(n)\times\sin(\Delta\omega_n n) = \frac{1}{2}E_s(n)E_o(n)\{\sin[2\Delta\omega_n n+\varphi_s(n)]-\sin\varphi_s(n)\}, \quad (2)$$

where $E_s(n)$ and $E_o(n)$ represent the electric field strength of the scattered light signal and the local oscillating signal at time point n, respectively, and $\varphi_s(n)$ represents the phase of the scattered light signal.

The sum frequency terms $\cos[2\Delta\omega_n n+\varphi_s(n)]$ and $\sin[2\Delta\omega_n n+\varphi_s(n)]$ in the I and Q signals, whose frequencies are two times of the frequency shift of the acousto-optic modulator (AOM), can be filtered out by the low-pass filter. After filtering, we can obtain $\cos\varphi_s(n)$ and $\sin\varphi_s(n)$ which contain the information of the external perturbation. The relationship between I, Q and $\cos\varphi_s(n)$, $\sin\varphi_s(n)$ exists as follows:

$$I \propto E_s(n)E_o(n)\cos\varphi_s(n), \quad (3)$$

$$Q \propto E_s(n)E_o(n)\sin\varphi_s(n). \quad (4)$$

Thus, the amplitude information of $S(n)$ is obtained as follows:

$$E_s(n)E_o(n) \propto \sqrt{I^2+Q^2}. \quad (5)$$

By processing the signal with moving average and moving difference, we can obtain a curve that represents the change in signal strength. At locations where the vibration changes strongly, there will be distinct vibration peaks indicating the exact location where the vibration occurs. According to the above equation, by performing the inverse tangent processing on the I and Q signals, we can obtain

$$\varphi_s(n) = -\arctan(\frac{Q}{I}+2k\pi), \quad (6)$$

where k is an integer. At this point, the value domain of the extracted phase information is limited between $(-\pi/2, \pi/2)$, while the actual external perturbation may exceed this range, leading to errors in the results after the inverse tangent. In order to obtain the correct phase information of the vibration signal, operations such as inverse tangent, value domain extension, and phase unwinding are required, and then the correct phase curve is obtained. The original vibration curve can be restored by extracting multiple phase points at the same location of the phase curve and performing a temporal unwinding process. The frequency information of the original vibration signal can be obtained by performing Fourier transform processing on the original vibration signal[20]. This series of processing steps ensures that we can accurately extract and analyze the signal changes caused by external perturbations, and then effectively monitor and locate the vibration events.

Due to the limitation of the pulse width of the light source and the processing rate of the data terminal, the measurement length, positioning accuracy, frequency response range, response speed and other indicators of the system are constrained by each other. After single optimization, the measurement length is more than 30 km, the positioning accuracy is better than ±1.8 m at 1 km, and the response time is less than 400 ms, where the response time refers to the time of completing the positioning demodulation, i.e., the time delay between the vibration source contacting with the measured optical fiber and applying the vibration signal, and the display of the first frame of the peak vibration curve on the monitoring interface. In order to investigate its response range to the frequency of vibration signals, an experimental measurement study was carried out to simulate variable frequency vibration signals. A piezoelectric ceramic tube with a diameter of 44 mm and a height of 40 mm is used as the simulated vibration source for testing, and a 20-m-long SMF-28e single-mode optical fiber is tightly wound on the outer surface of the PZT and glued with quick-drying adhesive to ensure that the vibration signals are effectively transmitted to the fiber; the fiber is fusion spliced to the end of the 1-km-long fiber to be tested, and then connected to the phase-sensitive optical time-domain reflectance system; the generator is used to load sinusoidal waveforms with different frequencies to the PZT, and the signal generator is used to measure the response to the vibration signals. The signal generator is used to load different frequencies of sine waves into the PZT to observe the changes of the system signal at the vibration position of the fiber end. Considering that there are about 100 m of redundant fibers +1 km fiber tray +20 m of fibers to be tested inside the module, a point near 1 120 m is selected as the reference for time-frequency demodulation of the vibration signal. The signal generator was adjusted to load vibration signals from 5 Hz to 25 kHz on the PZT, and as shown in Fig.3, the system observed the time-domain signals and frequency peaks of the typical vibration signals of 5 Hz, 30 Hz, 100 Hz, 200 Hz, 400 Hz, and 25 kHz, which were kept in perfect agreement with the real-time loaded vibration signals. The time-domain reduction and frequency-domain demodulation of the localization point show that the system is able to accurately locate the vibration signals within a wide range from 5 Hz to 25 kHz, ensuring that the original characteristics of the signals can meet the requirements of conventional vibration monitoring.

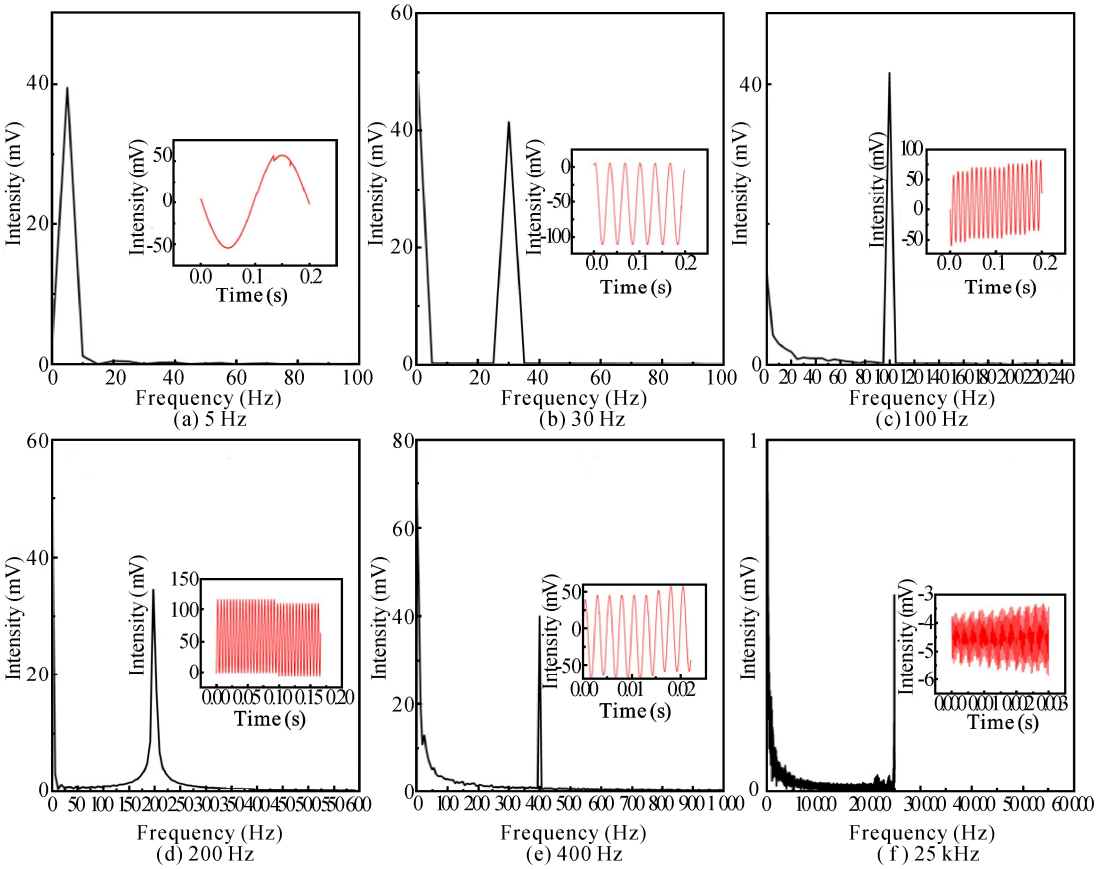

Fig.3 Different frequency sine wave spectra

As shown in Fig.4(a), the system was deployed in the 3D printed bridge on the campus of Hebei University of Technology to simulate the monitoring of bridge vibration. The field experiments were divided into three test areas to simulate three common vibration behaviors, such as walking, knocking, climbing, etc, with the spanning line laying, S type laying, and stone fence hanging net, respectively, and the results were analyzed and discussed in detail. First of all, as shown in Fig.4(c), spanning the diameter line laid fiber in the unimposed human disturbance and the external environment is relatively quiet, the vibration distribution curve amplitude of the whole fiber only shows the bottom noise curve. Fig.4(d) shows that when there is a significant wind disturbance in the external environment, the bridge deck laying of about 100 m of optical fiber produces a weak vibration response of 100 mV, and the front end of the fiber optic box of about 1 km of the tied fiber is not affected by the wind vibration. Fig.4(e) shows that when there are significant wind disturbance, the bridge deck laying of about 100 m optical fiber produced 100 mV weak vibration response, and about 1 km fiber box tied fiber did not suffer the wind vibration. Fig.4(e) shows the simulation of human walking vibration location appears significant single vibration peak, and the amplitude of nearly 500 mV is much larger than the fiber fluctuations caused by wind blowing. The above results show that by analyzing the difference in vibration intensity displayed by the system, it is possible to distinguish between the interference caused by ambient wind and the vibration caused by human interference.

In addition, as shown in Fig.5(a), two sections of fiber optic rings with an interval of 5 m were deployed on the bridge fence, and each fiber optic ring with 20 turns had a single-loop length of about 50 cm for a total of 10 m. The fiber optic samples were simply bonded to the stone bridge fence as a validation of the climbing behavior. When touching climbing points 1 and 2 individually, the system response is shown as black and red curves, respectively, and the touch signals of the two marked points can be recognized from the spatial location. Due to the long length and small spacing of the sample fibers, the vibration signal peaks of both are wider and there is obvious to be stickiness. When the climbing behavior at the same time touching the two measurement points, the system response as shown in the blue curve of the vibration signal appears split phenomenon, indicating that through the search peaks can distinguish two independent intrusion events and their localization. The inset of Fig.5(a) shows that the second deconvolution of the time domain reflects the significant time-domain intensity signal changes caused by the behavior of the climbing species, and the frequency spectrum is solved by the Fourier transform of the signal at a frequency of about 2.5 Hz.

Finally, as shown in Fig.5(b), the 3D-printed bridge was laid with about 50 m of 900 μm loose-casing sensing

fibers in an S-shaped arrangement, with a width of about 3.2 m at the end of the measurement fibers and a spacing of about 0.3 m in the direction of the spanning diameter line. This S type laying method is used instead of the straight line laying method in the direction of the bridge span line to obtain a higher spatial resolution, and the total length of 50 m of measurement fiber is laid in the bridge span of about 10 m. The physical distance between the bridge decks is about 1 m, and the total length of the measurement fiber is about 1.5 m. At this time, the physical distance between the bridge deck is approximately 1.8 m at two specific points. These points are connected by an S type fiber with a length of 10 m. According to the resolution definition for the 10-m-long optical fiber, it corresponds to a geometric distance of 1.8 m on the bridge deck. This is considered the equivalent spatial resolution for the deck. Consequently, the system can distinguish between vibrations at these two points, which are 1.8 m apart. However, employing this setup reduces the measurement range to one-fifth of its original extent. As illustrated, the two measurement points, separated by an actual spatial distance of about 1.8 m, are labeled as point A (proximal point) and point B (distal point). The fiber segment near these points is subjected to a frequency of about 5 Hz. This can be done either sequentially or simultaneously, targeting a length of approximately 50 cm. The process enables the spatial localization of two vibration sources, which are observed and differentiated simultaneously. The system response when tapping the fiber at point A and point B individually is shown in black and red curves, respectively, which can visually distinguish the positional difference between the two sources spatially. When the system response is shown in the blue curve when tapping point A and point B at the same time, the spatial positioning of the two vibration sources at the same time is exactly the same as when they act alone, and the adjacent fiber between point A and point B is not interfered with. The spatial resolution can be increased to 1.8 m at the expense of the measurement length by following the S shape of fiber placement, and it shows that the system is able to identify multiple vibration events independently without interfering with each other. The inset of Fig.5(b) shows the fluctuation of the intensity signal in the time domain caused by the knocking behavior, and the frequency domain analysis of the Fourier transform of the signal also shows that the vibration frequency of the knocking is about 5—10 Hz.

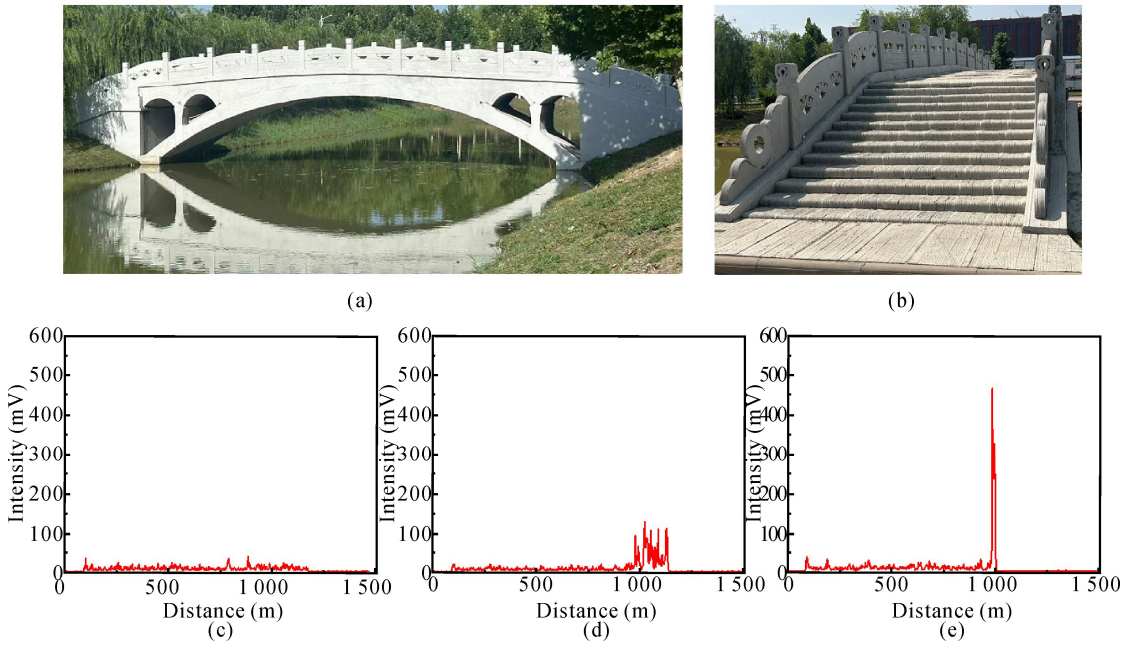

Fig.4 (a) Panoramic view of the bridge; (b) Front view of the bridge; (c) Vibration curve without disturbance; (d) Wind vibration curve; (e) Walking vibration curve

Through experimental studies, it is known that the system is able to collect three typical perturbation behaviors applied to 3D printed bridges in a highly sensitive manner. Whether it is from a single vibration source or multiple vibration sources acting in synchronization, the system is able to distinguish and accomplish precise positioning in a rapid and accurate manner. This provides a very promising technical support for the future monitoring and maintenance of bridge structures. The system's excellent frequency response characteristics cover a wide frequency range from 5 Hz to 25 kHz. This allows the system to localize in real time and accurately at multiple points, identifying the type of disturbance and frequency band. More importantly, the frequency range fully covers the frequency range of resonant vibrations that can lead to safety hazards and damage to the quality of bridges, which in the future can assist managers in taking protective measures to safeguard large infrastructures, such as bridges.

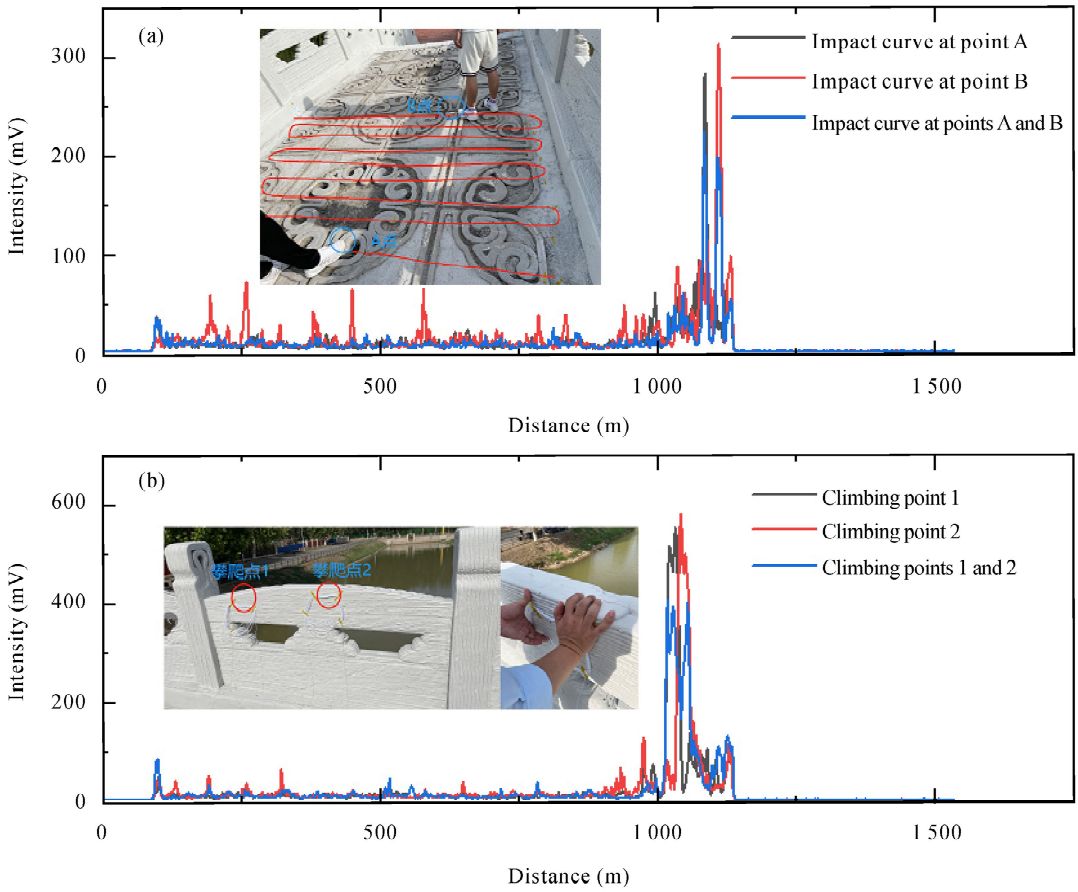

Fig.5 (a) Climbing vibration curve; (b) Tapping vibration curve

In our nuanced analysis of the experimental outcomes, we've taken a closer look at the system's nuanced response to a spectrum of vibrational events. Its ability to discern a single interaction across a 1.8-m-long fiber segment not only highlights the system's precision in identifying specific locations but also demonstrates its capability to reliably monitor the structural health of 3D printed bridges under practical conditions. The system's wide frequency response, covering from 5 Hz to 25 kHz, offers a comprehensive ability to detect a wide range of vibrational sources, attributable to both natural and human-induced factors.

In comparison with established vibration monitoring techniques, such as electronic vibration sensors, the φ-OTDR system we have introduced exhibits distinct advantages. Its robustness against electromagnetic interference, along with its proficiency in covering vast distances with minimal maintenance, suggests the φ-OTDR technology as a well-suited option for detailed, enduring assessments of structural health. The deliberate adoption of an S type layout enhances the system's resolution in space, a consideration that extends the granularity with which the system can perceive minor alterations in specific areas of the bridge.

4. Conclusion

In this study, a distributed fiber-optic sensing system based on φ-OTDR is experimentally verified to exhibit good accuracy and reliability in vibration monitoring of 3D printed bridges. The system is capable of responding to a single touch event at a distance of 1.8 m apart and accurately resolving vibration signals from 5 Hz to 25 kHz in the frequency domain and restoring them in the time domain. In the experiments, long-distance, multi-point and high-resolution vibration monitoring and information reduction were achieved by using fiber-optic S-shaped deployment on the bridge deck, the laying of spanning lines and the simulation of fence-hanging nets. These results indicate that the system has a wide range of potential applications and can be applied to all types of building infrastructure.

Future research can explore a wider range of application scenarios, such as vibration monitoring in other infrastructure areas such as tunnels and underground. At the same time, the performance of the system can be further optimized to improve the positioning accuracy and signal reduction capability to meet more demanding monitoring needs. In addition, the overall performance and reliability of the system can be further enhanced by combining other sensing technologies and algorithms. These efforts will provide more reliable structural health monitoring data support for the design, construction, operation and maintenance of intelligent building infrastructure, and make significant contributions to

safeguarding public safety and improving engineering efficiency.

Ethics declarations

Conflicts of interest

The authors declare no conflict of interest.

References

[1] BUSWELL R A, DA SILVA W R L, BOS F P, et al. A process classification framework for defining and describing digital fabrication with concrete[J]. Cement and concrete research, 2020, 134: 106068.

[2] BUCHLI J, GIFTTHALER M, KUMAR N, et al. Digital in situ fabrication-challenges and opportunities for robotic in situ fabrication in architecture, construction, and beyond[J]. Cement and concrete research, 2018, 112: 66-75.

[3] BAI G, WANG L, MA G, et al. 3D printing eco-friendly concrete containing under-utilized and waste solids as aggregates[J]. Cement and concrete composites, 2021, 120: 104037.

[4] DE SCHUTTER G, LESAGE K, MECHTCHERINE V, et al. Vision of 3D printing with concrete-technical, economic and environmental potentials[J]. Cement and concrete research, 2018, 112: 25-36.

[5] KONTOVOURKIS O, TRYFONOS G. Robotic 3D clay printing of prefabricated non-conventional wall components based on a parametric-integrated design[J]. Automation in construction, 2020, 110: 103005.

[6] FURET B, POULLAIN P, GARNIER S. 3D printing for construction based on a complex wall of polymer-foam and concrete[J]. Additive manufacturing, 2019, 28: 58-64.

[7] WANG L, MA G, LIU T, et al. Interlayer reinforcement of 3D printed concrete by the in-process deposition of U-nails[J]. Cement and concrete research, 2021, 148: 106535.

[8] HUBBARD P G, XU J, ZHANG S, et al. Dynamic structural health monitoring of a model wind turbine tower using distributed acoustic sensing (DAS)[J]. Journal of civil structural health monitoring, 2021, 11(3): 833-849.

[9] ZHAO H, DING Y, LI A, et al. State-monitoring for abnormal vibration of bridge cables focusing on non-stationary responses: from knowledge in phenomena to digital indicators[J]. Measurement, 2022, 205: 112148.

[10] WANG Y, YUAN H, LIU X, et al. A comprehensive study of optical fiber acoustic sensing[J]. IEEE access, 2019, 7: 85821-85837.

[11] TABJULA J, SHARMA J. Feature extraction techniques for noisy distributed acoustic sensor data acquired in a wellbore[J]. Applied optics, 2023, 62(16): E51-E61.

[12] SHANG Y, YANG Y, WANG C, et al. Optical fiber distributed acoustic sensing based on the self-interference of Rayleigh backscattering[J]. Measurement, 2016, 79: 222-227.

[13] NI J, WANG C, SHANG Y, et al. Distributed fiber-optic acoustic sensing for petroleum geology exploration[J]. Journal of physics: conference series, 2018, 1065: 252029.

[14] WANG Y, WANG X J, LI X L. OTDR-based optical fiber bending and tensile loss analysis[J]. Optoelectronics letters, 2023, 19(3): 164-169.

[15] PENG F, WU H, JIA X H, et al. Ultra-long high-sensitivity Φ-OTDR for high spatial resolution intrusion detection of pipelines[J]. Optics express, 2014, 22(11): 13804-13810.

[16] FERNÁNDEZ-RUIZ M R, SOTO M A, WILLIAMS E F, et al. Distributed acoustic sensing for seismic activity monitoring[J]. APL photon, 2020, 5: 030901.

[17] HUANG M F, JI P, WANG T, et al. First field trial of distributed fiber optical sensing and high-speed communication over an operational telecom network[J]. Journal of lightwave technology, 2020, 38: 75-81.

[18] WANG Z, ZHANG L, WANG S, et al. Coherent Φ-OTDR based on I/Q demodulation and homodyne detection[J]. Optics express, 2016, 24(2): 853-858.

[19] ZHANG P, VENKETESWARAN A, WRIGHT R, et al. Feature extraction for pipeline defects inspection based upon distributed acoustic fiber optic sensing data[J]. Fiber optic sensors and applications XVIII, 2022, 12105: 14-29.

[20] ZHOU R, ZHAO S, LUO M, et al. MFCC based real-time speech reproduction and recognition using distributed acoustic sensing technology[J]. Optoelectronics letters, 2024, 20(4): 222-227.